CAMx-UNIPAR Simulation of SOA Mass Formed from Multiphase Reactions of Hydrocarbons under the Central Valley Urban Atmospheres of California

5 Yujin Jo[1], Myoseon Jang[1], Sanghee Han[1], Azad Madhu[1], Bonyoung Koo[2], Yiqin Jia[2], Zechen Yu[1], Soontae Kim[3], and Jinsoo Park[4]

[1]Department of Environmental Engineering Sciences, Engineering School of Sustainable Infrastructure and Environment, University of Florida, Gainesville, FL, USA.
[2] Bay Area Air Quality Management District, San Francisco, CA, USA.
10 [3] Department of Environmental and Safety Engineering, Ajou University, Suwon, South Korea.
[4]Air Quality Research Division, National Institute of Environmental Research, Environmental Research Complex, Incheon, South Korea.

Correspondence to: Myoseon Jang (mjang@ufl.edu)

15 **Abstract.** The UNIfied Partitioning-Aerosol phase Reaction (UNIPAR) model was established on the Comprehensive Air quality Model with extensions (CAMx) to process Secondary Organic Aerosol (SOA) formation by capturing multiphase reactions of hydrocarbons (HCs) in regional scales. SOA growth was simulated using a wide range of anthropogenic HCs including ten aromatics and linear alkanes with different carbon-lengths. The atmospheric processes of biogenic HCs (isoprene, terpenes, and sesquiterpene) were simulated for the major

20 oxidation paths (ozone, OH radicals, and nitrate radicals) to predict day and night SOA formation. The UNIPAR model streamlined the multiphase partitioning of the lumping species originating from semi-explicitly predicted gas products and their heterogeneous chemistry to form non-volatile oligomeric species in both organic aerosol and inorganic aqueous phase. The CAMx-UNIPAR model predicted SOA formation at four ground urban sites (San Jose, Sacramento, Fresno, and Bakersfield) in California, United States during wintertime 2018. Overall, the simulated

25 mass concentrations of the total organic matter, consisting of primary OA (POA) and SOA, showed a good agreement with the observations. The simulated SOA mass in the urban areas of California was predominated by alkane and terpene. During the daytime, low-volatile products originating from the autoxidation of long-chain alkanes considerably contributed to the SOA mass. In contrast, a significant amount of nighttime SOA was produced by the reaction of terpene with ozone or nitrate radicals. The spatial distributions of anthropogenic SOA associated

30 with aromatic and alkane HCs were noticeably affected by the southward wind direction owing to the relatively long lifetime of their atmospheric oxidation, whereas those of biogenic SOA were nearly insensitive to wind direction. During wintertime 2018, the impact of inorganic aerosol hygroscopicity on the total SOA budget was not evident because of the small contribution of aromatic and isoprene products that are hydrophilic and reactive in the inorganic aqueous phase. However, an increased isoprene SOA mass was predicted during the wet periods, although

35 its contribution to the total SOA was little.

1 Introduction

Secondary Organic Aerosol (SOA) contributes a significant portion of Particulate Matter (PM) burden globally, with adverse impacts on health (Pye et al., 2021), visibility (Liu et al., 2022), and climate (Hallquist et al., 2009; Mahrt et al., 2022). SOA forms via gas–particle partitioning (Odum et al., 1996) of oxygenated products formed from the photooxidation of various hydrocarbons (HCs). Additionally, heterogeneous chemistry of oxidized carbons in the aerosol phase significantly contributes to SOA growth by forming non-volatile oligomeric mass (Hallquist et al., 2009; Kalberer et al., 2004; Tolocka et al., 2004). In particular, the contribution of heterogeneous chemistry on SOA mass increases with the aerosol water content associated with the hygroscopicity of electrolytic inorganic aerosol (Volkamer et al., 2009) and aerosol acidity (Jang et al., 2002).

The SOA model has been simulated in regional and global scales to predict the contribution of SOA mass to the total atmospheric organic aerosol (Zhang et al., 2021; Hodzic et al., 2015). The prediction of SOA formation has been approached by a conventional gas/particle partitioning of surrogate products (Odum et al., 1996) or the volatility basis set (VBS) approach (Donahue et al., 2006). However, these partitioning-based models poorly integrate the heterogeneous reactions of multifunctional organic products. The current models include isoprene but have no features for aqueous reactions of various products originating from various HCs (Vasilakos et al., 2021; Yu et al., 2022). Evidently, the limitation in the heterogeneous chemistry of various products can lead to deviations in the predicted SOA mass concentration from observations (Baker et al., 2015; Hayes et al., 2013; Carlton and Baker, 2011). For example, SOA formation has been underestimated in highly humid regions such as the Southeastern United States (US), in summer when the hygroscopic inorganic aerosol is wet (Zhang et al., 2018) and increases aqueous reactions of reactive organic species. To compensate the underestimation of SOA, the SOA model employed high partitioning-base model parameters, emerging gas mechanisms to form low-volatile products via autoxidation (Mayorga et al., 2022; Jokinen et al., 2015; Pye et al., 2019), or nighttime oxidations of HC with nitrate radical and ozone (Zaveri et al., 2020; Gao et al., 2019). These model parameters and reactions can improve SOA predictions but they can lead overprediction of SOA under certain situations. For example, Liu et al. (2021) reported in their regional simulation using the Community Earth System Model (CESM2.1) that the model parameters in the VBS model were too high for terpenes and led to overprediction of SOA mass with biased parameters that can overpredict organic matter (OM) mass (Liu et al., 2021).

The UNIfied Partitioning-Aerosol phase Reaction (UNIPAR) model predicts SOA mass by employing the multiphase partitioning of organic species between gas, organic and inorganic phases with improved prediction of thermodynamic parameters (i.e., activity coefficients of organic species in the salted inorganic phase under various humidity conditions) and in-particle chemistry (Beardsley and Jang, 2016; Im et al., 2014; Yu et al., 2021c; Zhou et al., 2019). Volatility-reactivity based lumping species originating from explicit gas mechanisms allow to estimate their physicochemical parameters that process multiphase partitioning and in-particle reactions (i.e., oligomerization and acid catalyzed reactions). The model parameters and equations established on UNIPAR have been demonstrated for various SOA originating from a wide range of HCs such as isoprene, terpenes, aromatics, and gasoline and demonstrated through chamber data under different levels of NO_x and different types of inorganic aerosols

associated with aerosol's acidity, hygroscopicity, and phase states (i.e., dry and wet) (Im et al., 2014; Beardsley and Jang, 2016; Cao and Jang, 2010; Zhou et al., 2019; Yu et al., 2021c; Han and Jang, 2022).

In a recent study by Yu et al. (2022), the UNIPAR model was integrated with the Comprehensive Air Quality Model
75 with extensions (CAMx) (Environ, 2020) and demonstrated its predictability of SOA mass for South Korea during the Korea-United States Air Quality (2016 KORUS-AQ) campaign. The CAMx–UNIPAR model well captured the prediction of SOA formation through the processing of aqueous phase reactions of organics and their gas-aqueous partitioning during wet periods during the KORUS-AQ campaign. Although the OM mass predicted with CAMx– UNIPAR was noticeably better than that of the CAMx model with the conventional partitioning-based two-product
80 model, the OM mass was somewhat underestimated compared with the observations. The underestimated OM was possibly due to missing precursors and missing chemistry in both the gas and aerosol phases.

In this study, the CAMx–UNIPAR model was extended to alkane SOA and nighttime chemistry of biogenic HCs. Long-chain alkanes are regarded as essential precursors for SOA formation (Aumont et al., 2012; Madhu et al., 2022). Studies have shown that the formation of low volatility products via peroxy radical autoxidation significantly
85 attributed to terpene SOA mass (Xavier et al., 2019; Bianchi et al., 2019). Madhu et al. (2022) recently extended an autoxidation mechanism to alkane semi-explicit oxidation mechanisms, improving the predictability of alkane SOA using the UNIPAR model against their chamber study. In addition, the UNIPAR model has recently been expanded to simulate biogenic SOA based on three major paths (i.e., OH radicals, ozone and nitrate radicals) being capable of nighttime SOA formation (Han and Jang, 2023) that was dominated by oxidation with ozone and nitrate radicals.
90 The performance of the extended CAMx–UNIPAR model of this study was demonstrated to predict the SOA budget under urban environments in the Central Valley, California (CA), US during the winter (January–February) in 2018. The impact of aerosol hygroscopicity on SOA formation under varied humidity conditions, spatial distributions of each SOA species, and diurnal patterns of SOA formation associated with nighttime oxidation of biogenic HCs were characterized using the CAMx–UNIPAR simulation in California's urban environments.

95 **2 Methods**

2.1 The UNIPAR SOA model

The structure of the UNIPAR SOA model has been described previously (Cao and Jang, 2010; Im et al., 2014; Beardsley and Jang, 2016; Zhou et al., 2019; Yu et al., 2021c; Yu et al., 2022; Choi and Jang, 2022; Madhu et al., 2022; Han and Jang, 2023). Briefly, the key components of the UNIPAR model are described as follow:
100 1) The SOA mass forms via multiphase partitioning, organic-phase oligomerization, and aqueous reactions in a wet inorganic salted solution. For the SOA formation in multiphase, a fundamental assumption is that organic constituents are internally mixed with inorganic constituents under the liquid-liquid phase separation between organic phase and salted aqueous phase.

2) As seen in Table 1, the 251 lumping groups in the current UNIPAR cover oxygenated products originating from
105 major 16 precursors (10 aromatics, three alkane groups in different carbon-lengths, isoprene, terpene, and sesquiterpene) with three major oxidation paths (OH radicals, ozone, and nitrate radicals) to represent HC oxidation

in day and night both. A pre-determined mathematical equation dynamically builds volatility-reactivity base 251 lumping arrays, which is connected to the stoichiometric coefficient array of oxygenated products predicted using explicit gas mechanisms (MCM v3.3.1(Jenkin, 2004)). These 251 lumping groups are applied to gas-particle partitioning and heterogeneous reactions to from SOA.

3) The mathematical equation for the stoichiometric coefficient array reflects the influence of NO_x levels and gas aging on gas-product distributions based on the RO_2 chemistry between RO_2+NO reactions and RO_2+HO_2 reactions under varying NO_x conditions day and night.

4) Lumping species' physicochemical parameters, such as molecular weight (MW_i), oxygen-to-carbon ratio ($O:C_i$), and hydrogen bonding (HB_i), are used to manage their multiphase partitioning. These physicochemical parameters are universalized for five major precursor groups in UNIPAR (Table 1). The physicochemical parameter arrays for MW_i, HB_i, and the $O:C_i$ ratios are reported in Tables S1–S3, respectively. The concentration of lumping species is distributed into gas (C_g), organic (C_{or}), and inorganic phases (C_{in}) using partitioning coefficients estimated based on Pankow's absorptive partitioning model (Pankow, 1994).

5)The kinetic parameters, such as lumping species' reactivity scales and their basicity constants, to calculate aerosol phase reaction rate constants in the organic phase and inorganic phase are reported in Tables S4–S5, respectively.

6) For the formation of non-volatile products, both organic phase oligomerization and aqueous reactions of reactive species yield non-volatile OM in the model. The lumping species in the lowest volatility is treated as non-volatile OM in this study. The SOA mass formed from gas-organic partitioning (OMP) is estimated using the Newtonian method (Schell et al., 2001) based on a mass balance of organic compounds between the gas and particle phases governed by Raoult's law. Heterogeneously formed non-volatile OM (OMH) are considered as a pre-existing absorbing material for gas-particle partitioning (Cao and Jang, 2010; Im et al., 2014).

7) To treat the SOA formation in the inorganic aqueous phase, the inorganic composition and aerosol acidity are predicted using inorganic thermodynamic model, ISORROPIA (Fountoukis and Nenes, 2007), and then incorporated into the UNIPAR model. Mutual deliquescence relative humidity (MDRH) is predicted from the ISORROPIA model. The efflorescence relative humidity (ERH) is predicted using a pre-trained neural network model based on the inorganic composition (Yu et al., 2021b). The aerosol state is determined to be wet (organic phase + inorganic aqueous phase) or dry (organic phase + solid-dry inorganic phase) with MDRH and ERH.

8) The formation of organosulfate in the form of dialkylsulfate, non-electrolytic and neutral ester of sulfuric acid with organic species, is reported in numerous laboratory studies (Liggio et al., 2005; Surratt et al., 2007; Li et al., 2015). In the model, the formation of dialkylsulfate is simulated by using the Hinshelwood-type reaction (Im et al., 2014). The decreased acidic sulfate due to the dialkylsulfate formation is applied to inorganic thermodynamic model (ISORROPIA) to calculate aerosol acidity and aerosol water content for the next step.

2.2 The CAMx-UNIPAR integration

Fig. 1 shows the overall structure of the CAMx-UNIPAR model. The Weather Research and Forecast model (WRF v4.1) generated meteorological input data to drive the CAMx v7.1 using the North American Mesoscale (NAM) data of the National Centers for Environmental Prediction (NCEP). The WRF modeling domains comprised three

nested grids with horizontal resolutions of 36, 12, and 4km. The outer domain, with a 36km horizontal resolution, covered the entire western US. The second domain, with a 12km horizontal resolution, covered California and

145 portions of Nevada. The third domain, with a 4km horizontal resolution, covered central California. The air quality simulation for gas and particle pollutants in central California was performed for the third domain (Fig. 2a) with 185×185 grids and 22 vertical layers. The detailed configurations of the WRF and CAMx modeling system are described in Table S6.

The UNIPAR SOA model was incorporated with the CAMx model as a sub-model to predict SOA formation in

150 California. Precursor HC consumption and other gas species were estimated using the SAPRC07TC gas mechanism (Hutzell et al., 2012) in the CAMx model. The inorganic thermodynamic model (ISORROPIA) provides the inorganic aerosol composition at equilibrium for inorganic aerosol species. The current CAMx-UNIPAR model includes 251 lumping species, of which 50 originate from ten aromatics; 50 originate from three alkane groups; 50 originate from terpene; 50 originate from sesquiterpene; and 51 originate from isoprene (Table 1).

155 In the model, three alkane groups with different carbon-chain lengths ranging from C9 to C24 were employed due to their different SOA formation potential. Speciation factor of 0.52 was used to estimate the emission of alkanes from SAPRC07TC ALK5, which contains other non-aromatic compounds (i.e., alcohols, ethers, esters, and carboxylic acids) in addition to alkanes (Carter, 2015). The emission factor of alkanes that were not fully covered by ALK5 (i.e., alkanes longer than C19, (Carter, 2015)) was estimated using the HC emission recently reported by the US

160 Environmental Protection Agency (US EPA) (Pye et al., 2022) and the study by Mcdonald et al. (2018). In this study, all types of alkanes including linear, branched, and cyclic alkanes were surrogated with linear alkanes based on a carbon number.

The SOA mass in the CAMx-UNIPAR model is attributed to the OMH and OMP for each precursor (Table 1). The total SOA is the sum of OMH_AR, OMH_AK, OMH_TE, OMH_SP, OMH_IS, OMP_AR, OMP_AK, OMP_TE,

165 OMP_SP, and OMP_IS. Total OM is the sum of total SOA and single primary organic aerosol (POA) species. POA is a single non-volatile species that does not chemically evolve (Environ, 2020). The simulation period was the winter (January–February) in 2018, excluding the wildfire season in California. Here, we focused on the simulation results that showed considerable OM levels between 01/23/2018 and 02/24/2018.

2.3 Observation sites in California

170 The US EPA has operated the national Chemical Speciation Monitoring Network (CSN) since 2000 to obtain information on the spatial and temporal chemical composition of ambient fine particles (Solomon et al., 2014). The CSN measures the major components of fine particles that are 2.5 microns or less in diameter ($PM_{2.5}$) including sulfate, nitrate, ammonium, organic carbon (OC) and elemental carbon (EC) and operates on a 1-in-3-day sample collection schedule. Fig. 2(a) shows four CSN sites in California - San Jose, Sacramento, Fresno, and Bakersfield

175 selected in this study. Table 2 summarizes information on the observation sites. The San Jose site is within the boundaries of the San Francisco Bay Area Air Basin (SFBAAB or Bay Area). The Sacramento, Fresno, and Bakersfield sites are located on flat land in the Central Valley. The Central Valley is bounded by mountain ranges

and coastal areas. This bowl-shaped geography of the Central Valley creates conditions conducive to holding pollutants in place and the accumulation of secondary photochemical compounds.

180 The Great Basin High occurred in California during the cold season (Herner et al., 2005). When the Great Basin High develops, the pressure gradients between the coast and the Central Valley decline, and the Planetary Boundary Layer (PBL) height becomes low. This condition holds pollutants close to the ground, allowing them to accumulate over several days, as fine particles and their precursors continue to be emitted. Due to a combination of unfavorable geographical and meteorological factors for ventilation, many cities in the bowl-shaped region, including San Jose,

185 Sacramento, Fresno, and Bakersfield, undergo persistent air quality issues (Lurmann et al., 2006; Young et al., 2016; Prabhakar et al., 2017; Chen et al., 2020; Sun et al., 2022).

2.4 Organic Carbon and Elemental Carbon data

The measured mass concentrations of EC at the San Jose, Sacramento, Fresno, and Bakersfield sites during the simulation period were used to separate the concentration of the measured total OC (OC_{tot}) into primary OC (POC)

190 and secondary OC (SOC) (Turpin and Huntzicker, 1995). Because EC and POC often have the same sources, there is a representative ratio of POC/EC for a given area (Strader et al., 1999). The POC is calculated based on Eq. 1 and the SOC is estimated by subtracting the resulting POC from the OC_{tot} as shown in Eq. 2 (Turpin and Huntzicker, 1995).

$$POC = EC \times \left(\frac{POC}{EC}\right) \tag{1}$$

195 $$SOC = OC_{tot} - POC \tag{2}$$

EC and OC_{tot} were measured from the same CSN system. In this study, the POC/EC ratio reported by Strader et al. (1999) by using field data obtained in California during the winter of 1995–1996 has been applied to estimate POC and SOC. The averaged POC/EC ratio was set to 2.4 with an upper limit of 2.75 and a lower limit of 2.05. OC_{tot} data, the estimated POC, and the estimated SOC were converted to total OM, POA, and SOA, respectively, using a

200 conversion factor of 1.7 (Mcdonald et al., 2015).

2.5 Emissions in California

The amounts of major SOA precursors - aromatics (ARO), alkane (ALK5), terpene (TERP), sesquiterpene (SESQ), and isoprene (ISOP) emissions for each site and the total of the domain are shown in Fig. 2(b). The spatial distributions of POA and major SOA precursors emissions for the California are shown in Fig. 2(c–h). The emission

205 data is SAPRC07-based and averaged between January and February in 2018. Aromatic emission is the sum of benzene, toluene, *o*-xylene, *p*-xylene, *m*-xylene, and 1,2,4-trimethylbenzene. The alkane corresponds to ALK5 in SAPRC07TC emission data.

On average, terpene, isoprene, alkane, aromatics, and sesquiterpene emissions in California accounted for 44, 31, 18, 7, and 1%, respectively, indicating the dominance of biogenic emissions, particularly terpene emissions, in

210 California. For the selected sites, alkane emissions accounted for more than 60%, followed by aromatic emissions at approximately 32%. Terpene and isoprene emissions accounted for less than 5%, and sesquiterpene emission was

negligible, indicating the dominance of alkane emissions in urban areas. Fig. 2(c–h) depicts a distinct difference in the spatial distribution of biogenic (terpene, sesquiterpene, and isoprene) and anthropogenic (POA, aromatics, and alkane) emissions. The spatial patterns of biogenic emissions followed the distribution of mountain ranges

215   surrounding the Central Valley, whereas the spatial patterns of POA, aromatics, and alkane emissions were concentrated in the source area such as industrial, transportation, and buildings in the Central Valley and Bay area. In addition, long-chain alkanes can also be attributed to biogenic sources. For example, alkanes are emitted from terrestrial higher plants cuticle wax, suspended spores, and aquatic plants, and they can be emitted to atmosphere during wildfire (Simoneit, 2002; Yao et al., 2009; Li et al., 2022).

220   **2.6 Meteorological variables**

The time series and scatter plots of the surface temperature, relative humidity, and wind speed simulated by the WRF model against observations at the four sites are shown in Figs. S1–S3, respectively, and their statistical summaries of correlation coefficient (R), Index of Agreement (IOA), and Mean Bias (MB) are described in Table S7. Detailed descriptions of these statistical parameters are presented in Table S8. Overall, the surface temperature,

225   relative humidity, and wind speed were well predicted with high R and IOA values, reducing uncertainties caused by the meteorological input data in the air quality simulation. Fig. S4 shows the wind rose plots for the four sites. Northwesterly winds prevailed at all sites, leading to the convergence of the pollutants in the southern area. Fig. S5 shows the time series of the hourly simulated PBL height at the four sites. The relatively low PBL height and weak wind speed appeared together in some periods (i.e., 01/26/2018 – 02/13/2018), creating conditions conducive to the

230   accumulation of pollutants.

In the CAMx-UNIPAR model, the phase state of inorganic aerosol is determined by using the calculated ERH based on the pre-trained neural network mathematical equation (Yu et al., 2021b) and the inorganic compositions (sulfate, nitrate, and ammonium) predicted from the inorganic thermodynamic model, ISORROPIA (Fountoukis and Nenes, 2007). The ERH and DRH of the salted aerosol and its phase state (wet or dry) is illustrated in Fig. S6. During the

235   simulation period, the inorganic aerosol phase was mostly wet, except for a few dry periods.

3 Results and Discussion

3.1 Simulation of organic matter

Fig. 3 shows the time series of the simulation of the total OM (Fig. 3a–d), POA (Fig. 3e–h), and SOA (Fig. 3i–l) with the CAMx-UNIPAR model against the observations at the four sites with statistical parameters (R, IOA, MB,

240   root mean square error (RMSE), and normalized MB (NMB) as described in Table S8. Overall, the simulated mass concentrations of total OM, consisting of POA and SOA, at four ground sites (San Jose, Sacramento, Fresno, and Bakersfield) showed a good agreement with the observations. The high R (0.77–0.89) and IOA values (0.82–0.87) in Fig. 3 indicate a good agreement between the predicted total OM and observed total OM concentrations. The marginally negative values for MB and NMB indicate that the model underestimated the total OM to some extent.

245   The simulation of the POA and SOA could capture observations, but it shows a marginal degradation in their R and IOA values compared with the total OM. The simulated POA was slightly overpredicted and the simulated SOA was somewhat underestimated at the four urban sites. Both MB and NMB values of POA were positive, while those of SOA were negative. The negative deviation of the predicted SOA is generally greater than the positive deviation of the POA, which affects the negative deviation of the total OM from the observations. The underestimation of

250   SOA mass can be attributed to missing precursor HCs and unidentified chemistry in the gas and aerosol phases. For example, the SOA model is currently missing phenols, branched and cyclic alkanes, and polyaromatic hydrocarbons (i.e., naphthalene). However, this statistical analysis may vary owing to the lack of observational data for the simulation periods. For example, the OC and EC observation data were only available for daily averaged data every three days (Sect. 2.3), and this low time-resolution observational data limited the verifications of the simulated OM

255   mass, especially SOA formation during daytime and nighttime from the CAMx-UNIPAR simulations. In addition, the observed POA estimated using the POC/EC ratio (Sect. 2.4) also has uncertainties because the POC/EC ratio is inconsistent from source to source but varies between sources (Strader et al., 1999).

The SOA/POA mass ratios estimated from the observation data ranged from 1.01 to 2.67 indicating a significant contribution of SOA mass to total OM. The simulated SOA/POA ratios were relatively lower than those in the

260   observed ratios, as discussed for the different deviations of the predicted POA and SOA from the observations. For both observations and simulation, the SOA fractions of the total OM in southern areas, such as Fresno and Bakersfield, were higher than those in northern areas, such as San Jose and Sacramento. The northern area, including the Bay Area is located on the upwind side of the southern area. A strong wind appeared in the northern area, decreasing the residence time of pollutants, which reduced secondary products of pollutants in this region. The

265   concentration of total OM, POA, and SOA increased from 01/23/2018 and maintained the high OM mass by early February. During this period, the wind speed was relatively weak (Fig. S3) and the PBL height was suppressed (Fig. S5), which is favorable for the accumulation of pollutants in urban areas.

3.2 Simulation of individual SOA species and their diurnal pattern

Fig. 4(a–d) shows the time series of the simulated POA and total SOA with the predicted salted aerosol phase state

270   (wet and dry) at the four sites. Both POA and SOA mass were noticeably high between 01/26/2018 and 02/13/2018, as discussed in sect. 3.1. Fig. 4(e–h) shows the time series of the simulated SOA species and pie charts to represent the averaged fraction of each SOA species during the period in Fig. 4. The predicted total SOA mass was predominated by alkane SOA (33–76%) and terpene SOA (18–60%) across all four sites. The contribution of alkane SOA and terpene SOA to the local SOA mass burden varied according to the location of the sites. For example, the

275   fraction of alkane SOA was higher than that of terpene SOA in all sites except Sacramento. The terpene concentrations can be high at the Sacramento site due to the proximity to the northern and eastern mountain ranges. Overall, the contributions of the isoprene SOA and aromatic SOA to the total SOA mass were small (~5%) and that of sesquiterpene SOA was nearly negligible.

A high fraction of OMP mass attributed to the total SOA as shown in Fig. 4(e–h). In particular, the alkane OMP

280   fraction of total SOA ranged from 20 to 41%, and the terpene OMP fraction of total SOA ranged from 15 to 53%. In

the current UNIPAR model, the low-volatile products produced from the oxidation of long-chain alkanes can significantly increases SOA growth via their gas-particle partitioning on the pre-existing OM. Additionally, the model includes the low volatility products originating from autoxidation of α-pinene ozonolysis products (Roldin et al., 2019; Crounse et al., 2013; Bianchi et al., 2019). The importance of autoxidation mechanisms on terpene SOA

285 formation was in a recent study by Yu et al. (2021c) for the daytime chemistry (Yu et al., 2021c).

In addition, the chamber study and the UNIPAR simulation by Han and Jang (2023) shows a significant potential for nighttime biogenic SOA formation (Han and Jang, 2023). In their study, α-pinene and isoprene SOA growth during nighttime is even more significant than their daytime growth due to the considerable contribution of both ozonolysis of biogenic HCs and the reaction with nitrate radicals, which yield low-volatile products. Ozone is produced via the

290 atmospheric oxidation of HCs integrated with a photochemical cycle of NO_x that prolongs through nighttime and promotes the formation of a nitrate radical in the presence of NO_2. This nitrate radical can attack an alkene in terpenes to form an alkylperoxy radical, leading to the formation of low-volatile peroxide accretion products (ROOR) (Hasan et al., 2021; Bates et al., 2022; Han and Jang, 2023).

The alkane OMH fractions of the total SOA ranged from 13 to 35%, which indicates that alkane OMH is still

295 significant, although less than alkane OMP. In the UNIPAR model, this alkane OMH is mainly associated with non-volatile products (extremely low-volatile products) originating from the autoxidation of long-chain alkanes. Unlike alkanes, other precursor HCs yield OMH via oligomerization of reactive semi-volatile organic species. Under California's 2018 winter simulation, the alkane OMH was larger than that sourced from non-alkane OMH. The attribution of autoxidation-driven low volatility products (alkane and terpene) to the total SOA mass can also

300 promote gas-particle partitioning of other products (non-autoxidation products), increasing the SOA mass.

Fig. 5 shows the diurnal variation of the fraction of SOA species, averaged between 01/23/2018 and 02/24/2018. The alkane SOA increased during the daytime because alkanes are mainly oxidized by reactions with an OH radical. As discussed above, terpene can be oxidized with an OH radical, a dominant oxidant in daytime, and furthermore terpene reacts with ozone and nitrate radicals during nighttime to form low volatility products, which can be a

305 significant source of OMP. The time series of the simulated concentrations of NO_2, ozone, and nitrate radicals are shown in Fig. S7. The time series of SOA precursor HCs (i.e., aromatic HCs, alkane, terpene, sesquiterpene, and isoprene) are shown in Fig. S8 and Fig. S9 shows those of SOA species. The terpene SOA mass at Fresno and Bakersfield noticeably increased (Fig. S9) between 01/29/2018 and 02/11/2018 when the concentrations of ozone and nitrate radicals were high (Fig. S7). During the simulation period, no specific fluctuations appeared in terpene

310 concentrations (Fig. S8), suggesting that terpene SOA formation is positively influenced by the concentrations of ozone and nitrate radicals.

3.3 Spatial distribution of SOA species

The surface-level spatial distributions of the total SOA, POA, and individual SOA species, averaged between 01/23/2018 and 02/24/2018, are displayed in Fig. 6. The spatial distribution of individual SOA species can be

315 influenced by the emission of each HC, available atmospheric oxidants, the reactivity of each HC with atmospheric oxidants, and winds (speed and direction). Fig. 2(c–h) illustrates the spatial distributions of the emission of POA and

each HC, and Fig. S10(a–c) shows those of NO_2 and atmospheric oxidants (ozone and nitrate radicals), respectively. The spatial distribution of the concentrations of each HC is shown in Fig. S10(d–h).

Biogenic HCs are rapidly consumed day and night due to their fast rate constants with OH radicals, ozone, and nitrate radicals and quickly form SOA. Hence, the spatial distributions of biogenic SOA were substantially influenced by the distribution of precursor HC emission sources and the long-range transport of particulates. As shown in Fig. 6(e), the terpene SOA mass was evenly distributed along the Central Valley, which was influenced by the high terpene emission from the surrounding mountains including the Cascade Range to the north, the Sierra Nevada to the east, and the Tehachapi Mountains to the south. On the other hand, the high NO_2 concentration appeared in urban areas of the Central Valley as shown in Fig. S10(a). Both ozone and nitrate radicals react with biogenic HCs to effectively form SOA via the production of low volatility products as discussed in Sect. 3.2 (Li et al., 2011; Jenkin, 2004; Han and Jang, 2023). The formation of nitrate radicals is favorable in urban areas because of the high concentrations of NO_2. Owing to the reaction of terpene with this nitrate radicals, the concentration of nitrate radicals was, however, low in the Central Valley. The maximum terpene SOA concentration appeared between the terpene ridge (Fig. S10f) and the NO_2 ridge (Fig. S10a) where the reaction rate between terpene and nitrate radicals was high. The sesquiterpene SOA distribution (Fig. 6f) was slightly southward compared with the terpene SOA distribution. In addition to emissions from mountain ranges, sesquiterpene can be sourced from various areas as shown in Fig. 2(g). California's isoprene emissions (Fig. 2h) are expected to originate from oak trees and from eucalyptus trees and are distributed in the central California foothills and South Coast Ranges. Thus, the isoprene SOA distribution was oriented more southward than that of the terpene SOA (Fig. 6g). Both sesquiterpene SOA and isoprene SOA were extremely small as discussed in Sect 3.2.

The spatial distributions of anthropogenic SOA were noticeably impacted by the southward wind direction. For example, the spatial distributions of both aromatic SOA (Fig. 6c) and alkane SOA (Fig. 6d) were extremely southward, although their emissions were relatively even along with the Central Valley (Fig. 2d and Fig. 2e). Unlike biogenic HCs, both aromatic and alkanes HCs have relatively a long lifetime for their atmospheric oxidation. Additionally, their major oxidation with OH radicals occurs in daytime. Thus, anthropogenic hydrocarbons can be transported along with the southward wind during the simulation period, which can increase the formation of anthropogenic SOA in the southern area. A $PM_{2.5}$ particle has an average lifetime of approximately eight days (Hodan and Barnard, 2004; Chowdhury et al., 2022). Noticeably, the POA also drifted to the south due to the transportation by the southward wind (Fig. 2c vs. Fig. 6b) and the high POA concentration augmented anthropogenic SOA growth in the southern area.

3.4 Impact of aerosol hygroscopicity on SOA formation

Numerous studies (Lim et al., 2010; Liu et al., 2012; Mcneill, 2015; Srivastava et al., 2022) have revealed that aqueous reactions of hydrophilic, reactive organic species in electrolytic inorganic aerosol produce non-volatile oligomeric matter and increase SOA mass. These heterogeneous reactions are known to be accelerated by acid catalyst species (Jang et al., 2002; Hallquist et al., 2009). In order to simulate the SOA formation potential by aerosol acidity at the four sites, the time series of hourly simulated concentrations of ionic species (sulfate, nitrate,

and ammonium in Fig. S11) were applied to estimate the aerosol acidity by the charge balance of the inorganic electrolytes. In Fig. S12, the charge balance estimated using the simulated and observed ionic concentrations suggested that the aerosol acidity was nearly neutral. The one-to-one line shown in Fig. S12 shows the fully titrated inorganic composition. Thus, SOA growth by the acid-catalyzed heterogeneous reactions of reactive lumping species might not have been effective during the simulation period of this study. Overall, nitrate concentrations in aerosol were high in the urban areas of California during the winter of 2018. The aerosols, which are enriched with ammonium nitrate salt, can be hygroscopic and lower the aerosol ERH and DRH (Fig. S6). As described in Sect. 2.6, the inorganic aerosol phase was mostly wet due to the low ERH and DRH with the abundant nitrate ammonium salt. The sensitivities of different SOA species to aerosol hygroscopicity are dissimilar. For example, aromatic and isoprene oxidation products are reactive for heterogeneous reactions and hydrophilic. Thus, they can effectively yield SOA in inorganic salted aqueous phase (Yu et al., 2021b). In contrast, both alkane and terpene oxidation products are relatively hydrophobic. Thus, their solubility in the aqueous phase is low due to their large activity coefficients. Evidently, α-pinene SOA and alkane SOA have a low O:C ratio (~0.55) (Zhang et al., 2015; Galeazzo et al., 2021; Madhu et al., 2022) compared with isoprene SOA (~1.1) (Song et al., 2015). In order to evaluate the sensitivity of different SOA species to aerosol hygroscopicity, the isoprene to alkane SOA mass ratios were calculated during the wet and dry periods as shown in Fig. 7. The SOA mass ratios of isoprene to alkane during the wet period were higher than those during the dry periods for all sites: San Jose, Sacramento, Fresno, and Bakersfield by factors of 3.0, 1.9, 2.8, and 2.0, respectively. Such high SOA mass ratios of isoprene to alkane during the wet period indicate the importance of the role of aerosol hygroscopicity on the SOA formation in an environment with a high emission of isoprene or aromatic HCs. The impact of aerosol hygroscopicity on SOA mass was minimal under California's atmospheric environment during the simulation period because of the dominance of alkane and terpene SOA. In contrast, the SOA mass simulated during the KORUS-AQ campaign was dominated by aromatic HCs, which produced reactive and hydrophilic products (Yu et al., 2022). In their study, the CAMx-UNIPAR model well captured a significant contribution of aromatic SOA to the total OM during the low-level transport/haze period (Crawford et al., 2021) where the aerosol water content was high.

4 Atmospheric Implications and uncertainties

The CAMx–UNIPAR model utilized 251 lumping species, which were constructed by using the semi-explicitly predicted products for three major oxidation paths (OH radicals, ozone, and nitrate radicals) of a wide range of HCs including aromatics, long-chain alkanes with different carbon lengths, isoprene, terpene, and sesquiterpene. Semi-explicit gas mechanisms captured the emerging chemistry in both the gas and aerosol phases as a function of the NO_x level and gas aging. In CAMx–UNIPAR, the calculation of the activity coefficient of lumping species in the multiphase allowed the simulation of the impact of temperature and humidity on the multiphase partitioning of lumping species and their heterogeneous reactions in the aerosol phase to form oligomeric OM. The OM budget was reasonably simulated by CAMx–UNIPAR for the urban environments in the Central Valley during the winter of 2018 (Fig. 3). However, the predicted POA was slightly overpredicted and the predicted SOA was somewhat underestimated compared with the decoupled POA and SOA from the observed OC.

11

390　In-depth analyses of individual SOA species in the Central valley under California's environment showed that the total SOA mass was predominated by daytime oxidation of long-chain alkanes ranging from C9–C24 and nighttime terpene oxidation with ozone and nitrate radicals (Sect. 3.2). SOA growth considerably increased with the low volatility products originating from the autooxidation of terpene and alkane oxidation products, and the nighttime chemistry of biogenic HCs. The prevalence of alkane and terpene SOA was the unique feature of California although their relative fractions to total OM may be switched seasonally. Unlike California, a significant SOA

395　species in East Asia was aromatic SOA because of the high emissions of aromatic HCs as seen in the CAMx–UNIPAR simulation during the KORUS-AQ campaign (Yu et al., 2022). We also concluded that the significance of inorganic hygroscopicity on SOA formation is influenced by the major SOA species. The aerosol's hygroscopicity effect on SOA formation is particularly pronounced in the region rich in isoprene or aromatic HC. Seemingly, the sensitivity of SOA formation to inorganic aerosol hygroscopicity in California was somewhat weaker than that

400　simulated in South Korea during the KROUS-AQ campaign. In the future, the CAMx–UNIPAR model needs to be demonstrated to predict SOA burdens in the Southeastern US, where isoprene is abundant due to its high emission from deciduous tree species (Palmer et al., 2003; Mauzerall et al., 2005) and it is humid, especially in summer.

An important feature of this study was the characterization of the influence of HC's atmospheric lifetime on the spatial distributions of each SOA species (Fig. 6). The simulated terpene SOA appeared in the region proximate to

405　terpene emission sources because of terpene's rapid oxidation day and night. Unlike terpene, the spatial distributions of aromatic and alkane HCs, which are relatively slowly oxidized in daytime with an OH radical, were influenced by the wind direction. Both alkane SOA and aromatic SOA were high in the south of the Central Valley due to the southward wind during wintertime. The similar tendency was simulated during the KORUS-AQ campaign (Yu et al., 2022). Aromatic HC emissions are high in the industrial areas of Shandong Province in East

410　China, and aromatic SOA was eastward along the wind direction. However, terpene SOA was almost synchronized with terpene sources, which were high from southeastern mountains in China.

Due to efforts by the government, NO_x and SO_2 emissions from anthropogenic sources have been gradually reduced (Winkler et al., 2018; Zheng et al., 2018; Yu et al., 2021a; Aas et al., 2019). The sensitivity of each SOA species to the NO_x level can be various according to their oxidation mechanisms. For example, chamber studies showed that

415　aromatic SOA yields increased with decreasing the NO_x level within the NO_x-rich region (Yang et al., 2020). A gradual increase in alkane SOA was reported in the recent chamber study by Madhu et al. (2022) with decreasing the NO_x level over both NO_x-rich and NO_x-poor regions. The reduction of NO_x in the NO_x-rich region dramatically decreases nighttime biogenic SOA yields owing to the reaction of biogenic HCs with decreased nitrate radicals, but the reduced NO_x increases daytime biogenic SOA yields (Han and Jang, 2023). In particular, the formation of the

420　low-volatile products formed via the autooxidation of ozonolysis products is an essential source of biogenic SOA as discussed by Pye et al. (2022). In polluted urban environments (NO_x-rich), the elevation of SOA mass with lowering NO_x might be more substantial in East Asia, where aromatic SOA is dominant than that in California, where terpene and alkane SOA are dominant. In the NO_x-poor region, the potential SOA rise by NO_x reduction may still occur in California because of negative correlation between alkane SOA and NO_x level over the entire NO_x range and the

425　contribution of autooxidation products from terpene and alkanes. The reduction of SO_2 drops aerosol acidity and

thus, it can lessen the SOA mass. SO_2 reduction may be beneficial in East Asia where aromatic SOA is dominant and the Southeastern US where isoprene SOA is important.

The possible uncertainties in the SOA simulation using the CAMx-UNIPAR model are associated with missing precursors, the classification of precursors due to uncertainties in emission data and the use of surrogates, and the mass balance between gas chemistry and the aerosol module. Numerous precursors are not involved in the SOA model because of the lack of emission data and model parameters of HCs such as phenols, branched and cyclic alkane, and polyaromatic hydrocarbons (i.e., naphthalene). In order to reduce the computational time, some HC classes use a surrogate compound. For example, α-pinene was a surrogate for all terpenes and this substitution causes uncertainties in terpene SOA due to the different reactivity to oxidants, the formation of autoxidation products and SOA yields (Yu et al., 2021c). In this study, all alkanes were surrogated by linear alkanes. Overall, branched alkanes can yield lower SOA yields than linear alkanes at a given carbon number, whereas cyclic alkanes can yield higher SOA yields. In this model, the carbon balance between gas chemistry and the aerosol module, which is caused by consumption of carbon to form SOA, has not been addressed. Pye et al. (2022) recently developed the Community Regional Atmospheric Chemistry Multiphase Mechanism (CRACMM v1.0), which employs explicit oxidized products to improve the carbon balance between gas mechanisms and the SOA model (Pye et al., 2022). Interconnecting atmospheric gas-chemistry with SOA formation is essential because SOA formation is a dynamic process as a function of precursors HCs, NO_x, SO_2, and atmospheric oxidants.

Code availability. Code to run the CAMx-UNIPAR model in this study is available upon request.

Data availability. Regional simulation input data is available upon request.

Author contributions. Y. Jo simulated the air quality by using the CAMx-UNIPAR model for the urban environments in the Central Valley, CA. Y. Jo and MJ interpreted the air quality simulation results. Y. Jo, MJ and ZY integrated the UNIPAR code and model parameters into CAMx. SH and AM produced model parameters for UNIPAR. BK and Y. Jia provided emission and meteorology inputs for California's air quality. SK and JP generated emission split factors for SOA precursors.

Competing interest. The authors declare that they have no conflict of interest.

References

460 Aas, W., Mortier, A., Bowersox, V., Cherian, R., Faluvegi, G., Fagerli, H., Hand, J., Klimont, Z., Galy-Lacaux, C., Lehmann, C. M. B., Myhre, C. L., Myhre, G., Olivie, D., Sato, K., Quaas, J., Rao, P. S. P., Schulz, M., Shindell, D., Skeie, R. B., Stein, A., Takemura, T., Tsyro, S., Vet, R., and Xu, X.: Global and regional trends of atmospheric sulfur, Sci. Rep., 9, 953, https://doi.org/10.1038/s41598-018-37304-0, 2019.

Aumont, B., Valorso, R., Mouchel-Vallon, C., Camredon, M., Lee-Taylor, J., and Madronich, S.: Modeling SOA
465 formation from the oxidation of intermediate volatility n-alkanes, Atmos. Chem. Phys., 12, 7577-7589, https://doi.org/10.5194/acp-12-7577-2012, 2012.

Baker, K. R., Carlton, A. G., Kleindienst, T. E., Offenberg, J. H., Beaver, M. R., Gentner, D. R., Goldstein, A. H., Hayes, P. L., Jimenez, J. L., Gilman, J. B., de Gouw, J. A., Woody, M. C., Pye, H. O. T., Kelly, J. T., Lewandowski, M., Jaoui, M., Stevens, P. S., Brune, W. H., Lin, Y. H., Rubitschun, C. L., and Surratt, J. D.: Gas and aerosol carbon
470 in California: comparison of measurements and model predictions in Pasadena and Bakersfield, Atmos. Chem. Phys., 15, 5243-5258, https://doi.org/10.5194/acp-15-5243-2015, 2015.

Bates, K. H., Burke, G. J., Cope, J. D., and Nguyen, T. B.: Secondary organic aerosol and organic nitrogen yields from the nitrate radical (NO_3) oxidation of alpha-pinene from various RO_2 fates, Atmos. Chem. Phys., 22, 1467-1482, https://doi.org/10.5194/acp-22-1467-2022, 2022.

475 Beardsley, R. L. and Jang, M.: Simulating the SOA formation of isoprene from partitioning and aerosol phase reactions in the presence of inorganics, Atmos. Chem. Phys., 16, 5993-6009, https://doi.org/10.5194/acp-16-5993-2016, 2016.

Bianchi, F., Kurten, T., Riva, M., Mohr, C., Rissanen, M., Roldin, P., Berndt, T., Crounse, J., Wennberg, P., Mentel, T., Wildt, J., Junninen, H., Jokinen, T., Kulmala, M., Worsnop, D., Thornton, J., Donahue, N., Kjaergaard, H., and
480 Ehn, M.: Highly Oxygenated Organic Molecules (HOM) from Gas-Phase Autoxidation Involving Peroxy Radicals: A Key Contributor to Atmospheric Aerosol, Chem. Rev., 119, 3472-3509, https://doi.org/10.1021/acs.chemrev.8b00395, 2019.

Cao, G. and Jang, M.: An SOA Model for Toluene Oxidation in the Presence of Inorganic Aerosols, Environ. Sci. Technol., 44, 727-733, https://doi.org/10.1021/es901682r, 2010.

485 Carlton, A. G. and Baker, K. R.: Photochemical modeling of the Ozark isoprene volcano: MEGAN, BEIS, and their impacts on air quality predictions, Environ. Sci. Technol., 45, 4438-4445, https://doi.org/10.1021/es200050x, 2011.

Carter, W. P.: Development of a database for chemical mechanism assignments for volatile organic emissions, J. Air Waste Manag. Assoc., 65, 1171-1184, https://doi.org/10.1080/10962247.2015.1013646, 2015.

Chen, J., Yin, D., Zhao, Z., Kaduwela, A. P., Avise, J. C., DaMassa, J. A., Beyersdorf, A., Burton, S., Ferrare, R.,
490 Herman, J. R., Kim, H., Neuman, A., Nowak, J. B., Parworth, C., Scarino, A. J., Wisthaler, A., Young, D. E., and Zhang, Q.: Modeling air quality in the San Joaquin valley of California during the 2013 Discover-AQ field campaign, Atmos. Environ. X, 5, https://doi.org/10.1016/j.aeaoa.2020.100067, 2020.

Choi, J. and Jang, M.: Suppression of the phenolic SOA formation in the presence of electrolytic inorganic seed, Sci. Total Environ., 851, 158082, https://doi.org/10.1016/j.scitotenv.2022.158082, 2022.

495   Chowdhury, S., Pozzer, A., Haines, A., Klingmuller, K., Munzel, T., Paasonen, P., Sharma, A., Venkataraman, C.,
       and Lelieveld, J.: Global health burden of ambient $PM_{2.5}$ and the contribution of anthropogenic black carbon and
       organic aerosols, Environ. Int., 159, 107020, https://doi.org/10.1016/j.envint.2021.107020, 2022.

       Crawford, J. H., Ahn, J. Y., Al-Saadi, J., Chang, L., Emmons, L. K., Kim, J., Lee, G., Park, J. H., Park, R. J., Woo, J.
       H., Song, C. K., Hong, J. H., Hong, Y. D., Lefer, B. L., Lee, M., Lee, T., Kim, S., Min, K. E., Yum, S. S., Shin, H. J.,
500   Kim, Y. W., Choi, J. S., Park, J. S., Szykman, J. J., Long, R. W., Jordan, C. E., Simpson, I. J., Fried, A., Dibb, J. E.,
       Cho, S., and Kim, Y. P.: The Korea-United States Air Quality (KORUS-AQ) field study, Elementa (Wash D C), 9,
       1-27, https://doi.org/10.1525/elementa.2020.00163, 2021.

       Crounse, J. D., Nielsen, L. B., Jørgensen, S., Kjaergaard, H. G., and Wennberg, P. O.: Autoxidation of organic
       compounds in the atmosphere, J. Phys. Chem. Lett., 4, 3513-3520, https://doi.org/10.1021/jz4019207, 2013.

505   Donahue, N. M., Robinson, A. L., Stanier, C. O., and Pandis, S. N.: Coupled Partitioning, Dilution, and Chemical
       Aging of Semivolatile Organics, Environ. Sci. Technol., 40, 2635-2643, https://doi.org/10.1021/es052297c, 2006.

       ENVIRON, R.: User's Guide Comprehensive Air Quality Model with Extensions version 7.10, 2020.

       Fountoukis, C. and Nenes, A.: ISORROPIA II: a computationally efficient thermodynamic equilibrium model for
       K^+-Ca^{2+}-Mg^{2+}-NH_4^+-Na^+-SO_4^{2-}-NO_3^--Cl^--H_2O aerosols,   Atmos.   Chem.   Phys.,   7,   4639-4659,
510   https://doi.org/10.5194/acp-7-4639-2007, 2007.

       Galeazzo, T., Valorso, R., Li, Y., Camredon, M., Aumont, B., and Shiraiwa, M.: Estimation of secondary organic
       aerosol viscosity from explicit modeling of gas-phase oxidation of isoprene and α-pinene, Atmos. Chem. Phys., 21,
       10199-10213, https://doi.org/10.5194/acp-21-10199-2021, 2021.

       Gao, S., Lathem, T., and Nyadong, L.: Nighttime secondary organic aerosol formation from unburned fuel vapors,
515   Atmos. Environ., 204, 125-134, https://doi.org/10.1016/j.atmosenv.2019.02.028, 2019.

       Hallquist, M., Wenger, J. C., Baltensperger, U., Rudich, Y., Simpson, D., Claeys, M., Dommen, J., Donahue, N. M.,
       George, C., Goldstein, A. H., Hamilton, J. F., Herrmann, H., Hoffmann, T., Iinuma, Y., Jang, M., Jenkin, M. E.,
       Jimenez, J. L., Kiendler-Scharr, A., Maenhaut, W., McFiggans, G., Mentel, T. F., Monod, A., Prévôt, A. S. H.,
       Seinfeld, J. H., Surratt, J. D., Szmigielski, R., and Wildt, J.: The formation, properties and impact of secondary
520   organic aerosol: current and emerging issues, Atmos. Chem. Phys., 9, 5155-5236, https://doi.org/10.5194/acp-9-
       5155-2009, 2009.

       Han, S. and Jang, M.: Prediction of secondary organic aerosol from the multiphase reaction of gasoline vapor by
       using volatility–reactivity base lumping, Atmos. Chem. Phys., 22, 625-639, https://doi.org/10.5194/acp-22-625-
       2022, 2022.

525   Han, S. and Jang, M.: Modeling daytime and nighttime secondary organic aerosol formation via multiphase
       reactions of biogenic hydrocarbons, Atmos. Chem. Phys., 23, 1209–1226, https://doi.org/10.5194/acp-23-1209-2023,
       2023.

       Hasan, G., Valiev, R. R., Salo, V.-T., and Kurtén, T.: Computational Investigation of the Formation of Peroxide
       (ROOR) Accretion Products in the OH-and NO_3-Initiated Oxidation of α-Pinene, J. Phys. Chem. A, 125, 10632-
530   10639, https://doi.org/10.1021/acs.jpca.1c08969, 2021.

Hayes, P. L., Ortega, A. M., Cubison, M. J., Froyd, K. D., Zhao, Y., Cliff, S. S., Hu, W. W., Toohey, D. W., Flynn, J. H., Lefer, B. L., Grossberg, N., Alvarez, S., Rappenglück, B., Taylor, J. W., Allan, J. D., Holloway, J. S., Gilman, J. B., Kuster, W. C., de Gouw, J. A., Massoli, P., Zhang, X., Liu, J., Weber, R. J., Corrigan, A. L., Russell, L. M., Isaacman, G., Worton, D. R., Kreisberg, N. M., Goldstein, A. H., Thalman, R., Waxman, E. M., Volkamer, R., Lin, Y. H., Surratt, J. D., Kleindienst, T. E., Offenberg, J. H., Dusanter, S., Griffith, S., Stevens, P. S., Brioude, J., Angevine, W. M., and Jimenez, J. L.: Organic aerosol composition and sources in Pasadena, California, during the 2010 CalNex campaign, J. Geophys. Res.-Atmos., 118, 9233-9257, https://doi.org/10.1002/jgrd.50530, 2013.

Herner, J. D., Aw, J., Gao, O., Chang, D. P., and Kleeman, M. J.: Size and composition distribution of airborne particulate matter in northern California: I – particulate mass, carbon, and water-soluble ions, J. Air Waste Manag. Assoc., 55, 30-51, https://doi.org/10.1080/10473289.2005.10464600, 2005.

Hodan, W. M. and Barnard, W. R.: Evaluating the Contribution of $PM_{2.5}$ Precursor Gases and Re-entrained Road Emissions to Mobile Source $PM_{2.5}$ Particulate Matter Emissions, 2004.

Hodzic, A., Madronich, S., Kasibhatla, P. S., Tyndall, G., Aumont, B., Jimenez, J. L., Lee-Taylor, J., and Orlando, J.: Organic photolysis reactions in tropospheric aerosols: effect on secondary organic aerosol formation and lifetime, Atmos. Chem. Phys., 15, 9253-9269, https://doi.org/10.5194/acp-15-9253-2015, 2015.

Hutzell, W. T., Luecken, D. J., Appel, K. W., and Carter, W. P. L.: Interpreting predictions from the SAPRC07 mechanism based on regional and continental simulations, Atmos. Environ., 46, 417-429, https://doi.org/10.1016/j.atmosenv.2011.09.030, 2012.

Im, Y., Jang, M., and Beardsley, R. L.: Simulation of aromatic SOA formation using the lumping model integrated with explicit gas-phase kinetic mechanisms and aerosol-phase reactions, Atmos. Chem. Phys., 14, 4013-4027, https://doi.org/10.5194/acp-14-4013-2014, 2014.

Jang, M., Czoschke, N. M., Lee, S., and Kamens, R. M.: Heterogeneous Atmospheric Aerosol Production by Acid-Catalyzed Particle-Phase Reactions, Science, 298, 814-817, https://doi.org/10.1126/science.1075798, 2002.

Jenkin, M. E.: Modelling the formation and composition of secondary organic aerosol from α- and β-pinene ozonolysis using MCM v3, Atmos. Chem. Phys., 4, 1741-1757, https://doi.org/10.5194/acp-4-1741-2004, 2004.

Jokinen, T., Berndt, T., Makkonen, R., Kerminen, V. M., Junninen, H., Paasonen, P., Stratmann, F., Herrmann, H., Guenther, A. B., Worsnop, D. R., Kulmala, M., Ehn, M., and Sipila, M.: Production of extremely low volatile organic compounds from biogenic emissions: Measured yields and atmospheric implications, P. Natl. Acad. Sci. USA, 112, 7123-7128, https://doi.org/10.1073/pnas.1423977112, 2015.

Kalberer, M., Paulsen, D., Sax, M., Steinbacher, M., Dommen, J., Prevot, A. S., Fisseha, R., Weingartner, E., Frankevich, V., Zenobi, R., and Baltensperger, U.: Identification of Polymers as Major Components of Atmospheric Organic Aerosols, Science, 303, 1659-1662, https://doi.org/10.1126/science.1092185, 2004.

Li, J., Jang, M., and Beardsley, R.: Dialkylsulfate Formation in Sulfuric Acid Seeded Secondary Organic Aerosol Produced Using an Outdoor Chamber Under Natural Sunlight, Environ. Chem., 13, 590-601, https://doi.org/10.1071/EN15129, 2015.

Li, J., Li, K., Li, H., Wang, X., Wang, W., Wang, K., and Ge, M.: Long-chain alkanes in the atmosphere: A review, J. Environ. Sci. (China), 114, 37-52, https://doi.org/10.1016/j.jes.2021.07.021, 2022.

Li, Y. J., Chen, Q., Guzman, M. I., Chan, C. K., and Martin, S. T.: Second-generation products contribute substantially to the particle-phase organic material produced by β-caryophyllene ozonolysis, Atmos. Chem. Phys., 570   11, 121-132, https://doi.org/10.5194/acp-11-121-2011, 2011.

Liggio, J., Li, S.-M., and McLaren, R.: Heterogeneous Reactions of Glyoxal on Particulate Matter: Identification of Acetals and Sulfate Esters, Environ. Sci. Technol., 39, 1532-1541, https://doi.org/10.1021/es048375y, 2005.

Lim, Y. B., Tan, Y., Perri, M. J., Seitzinger, S. P., and Turpin, B. J.: Aqueous chemistry and its role in secondary organic aerosol (SOA) formation, Atmospheric Chemistry and Physics, 10, 10521-10539, 10.5194/acp-10-10521-575   2010, 2010.

Lim, Y. B., Tan, Y., Perri, M. J., Seitzinger, S. P., and Turpin, B. J.: Aqueous chemistry and its role in secondary organic aerosol (SOA) formation, Atmos. Chem. Phys., 10, 10521-10539, https://doi.org/10.5194/acp-10-10521-2010, 2010.

Liu, L., Kuang, Y., Zhai, M., Xue, B., He, Y., Tao, J., Luo, B., Xu, W., Tao, J., Yin, C., Li, F., Xu, H., Deng, T., 580   Deng, X., Tan, H., and Shao, M.: Strong light scattering of highly oxygenated organic aerosols impacts significantly on visibility degradation, Atmos. Chem. Phys., 22, 7713-7726, https://doi.org/10.5194/acp-22-7713-2022, 2022.

Liu, Y., Dong, X., Wang, M., Emmons, L. K., Liu, Y., Liang, Y., Li, X., and Shrivastava, M.: Analysis of secondary organic aerosol simulation bias in the Community Earth System Model (CESM2.1), Atmos. Chem. Phys., 21, 8003-8021, https://doi.org/10.5194/acp-21-8003-2021, 2021.

585   Liu, Y., Siekmann, F., Renard, P., El Zein, A., Salque, G., El Haddad, I., Temime-Roussel, B., Voisin, D., Thissen, R., and Monod, A.: Oligomer and SOA formation through aqueous phase photooxidation of methacrolein and methyl vinyl ketone, Atmos. Environ., 49, 123-129, https://doi.org/10.1016/j.atmosenv.2011.12.012, 2012.

Lurmann, F. W., Brown, S. G., McCarthy, M. C., and Roberts, P. T.: Processes influencing secondary aerosol formation in the San Joaquin Valley during winter, J. Air Waste Manag. Assoc., 56, 1679-1693, 590   https://doi.org/10.1080/10473289.2006.10464573, 2006.

Madhu, A., Jang, M., and Deacon, D.: Modeling the Influence of Chain Length on SOA Formation via Multiphase Reactions of Alkanes, EGUsphere, 2022, 1-30, https://doi.org/10.5194/egusphere-2022-681, 2022.

Mahrt, F., Peng, L., Zaks, J., Huang, Y., Ohno, P. E., Smith, N. R., Gregson, F. K. A., Qin, Y., Faiola, C. L., Martin, S. T., Nizkorodov, S. A., Ammann, M., and Bertram, A. K.: Not all types of secondary organic aerosol mix: two 595   phases observed when mixing different secondary organic aerosol types, Atmos. Chem. Phys., 22, 13783-13796, https://doi.org/10.5194/acp-22-13783-2022, 2022.

Mauzerall, D., Sultan, B., Kim, N., and Bradford, D.: Charging NO_x Emitters for Health Damages: An Exploratory Analysis, SSRN Electronic Journal, https://doi.org/10.2139/ssrn.706782, 2005.

Mayorga, R., Xia, Y., Zhao, Z., Long, B., and Zhang, H.: Peroxy Radical Autoxidation and Sequential Oxidation in 600   Organic Nitrate Formation during Limonene Nighttime Oxidation, Environ. Sci. Technol., 56, 15337-15346, https://doi.org/10.1021/acs.est.2c04030, 2022.

McDonald, B. C., Goldstein, A. H., and Harley, R. A.: Long-term trends in California mobile source emissions and ambient concentrations of black carbon and organic aerosol, Environ. Sci. Technol., 49, 5178-5188, https://doi.org/10.1021/es505912b, 2015.

605 McDonald, B. C., de Gouw, J. A., Gilman, J. B., Jathar, S. H., Akherati, A., Cappa, C. D., Jimenez, J. L., Lee-Taylor, J., Hayes, P. L., McKeen, S. A., Cui, Y. Y., Kim, S. W., Gentner, D. R., Isaacman-VanWertz, G., Goldstein, A. H., Harley, R. A., Frost, G. J., Roberts, J. M., Ryerson, T. B., and Trainer, M.: Volatile chemical products emerging as largest petrochemical source of urban organic emissions, Science, 359, 760-764, https://doi.org/10.1126/science.aaq0524, 2018.

610 McNeill, V. F.: Aqueous organic chemistry in the atmosphere: sources and chemical processing of organic aerosols, Environ. Sci. Technol., 49, 1237-1244, https://doi.org/10.1021/es5043707, 2015.

Odum, J. R., Hoffmann, T., Bowman, R., Collins, D., Flagan, R. C., and Seinfeld, J. H.: Gas/Particle Partitioning and Secondary Organic Aerosol Yields, Environ. Sci. Technol., 1996.

Palmer, P. I., Jacob, D. J., Fiore, A. M., Martin, R. V., Chance, K., and Kurosu, T. P.: Mapping isoprene emissions
615 over North America using formaldehyde column observations from space, J. Geophys. Res.-Atmos., 108, https://doi.org/10.1029/2002JD002153, 2003.

Pankow, J. F.: An Absorption Model of the Gas/Aerosol Partitioning Involved in the Formation of Secondary Oorganic Aerosol, Atmos. Environ., 28, 189-193, https://doi.org/10.1016/1352-2310(94)90094-9, 1994.

Prabhakar, G., Parworth, C., Zhang, X., Kim, H., Young, D., Beyersdorf, A. J., Ziemba, L. D., Nowak, J. B.,
620 Bertram, T. H., Faloona, I. C., Zhang, Q., and Cappa, C. D.: Observational assessment of the role of nocturnal residual-layer chemistry in determining daytime surface particulate nitrate concentrations, Atmos. Chem. Phys., 17, 14747-14770, https://doi.org/10.5194/acp-17-14747-2017, 2017.

Pye, H. O. T., Ward-Caviness, C. K., Murphy, B. N., Appel, K. W., and Seltzer, K. M.: Secondary organic aerosol association with cardiorespiratory disease mortality in the United States, Nat. Commun., 12, 7215,
625 https://doi.org/10.1038/s41467-021-27484-1, 2021.

Pye, H. O. T., Place, B. K., Murphy, B. N., Seltzer, K. M., D'Ambro, E. L., Allen, C., Piletic, I. R., Farrell, S., Schwantes, R. H., Coggon, M. M., Saunders, E., Xu, L., Sarwar, G., Hutzell, W. T., Foley, K. M., Pouliot, G., Bash, J., and Stockwell, W. R.: Linking gas, particulate, and toxic endpoints to air emissions in the Community Regional Atmospheric Chemistry Multiphase Mechanism (CRACMM) version 1.0, Atmos. Chem. Phys. Discuss., 2022, 1-88,
630 https://doi.org/10.5194/acp-2022-695, 2022.

Pye, H. O. T., D'Ambro, E. L., Lee, B. H., Schobesberger, S., Takeuchi, M., Zhao, Y., Lopez-Hilfiker, F., Liu, J., Shilling, J. E., Xing, J., Mathur, R., Middlebrook, A. M., Liao, J., Welti, A., Graus, M., Warneke, C., de Gouw, J. A., Holloway, J. S., Ryerson, T. B., Pollack, I. B., and Thornton, J. A.: Anthropogenic enhancements to production of highly oxygenated molecules from autoxidation, P. Natl. Acad. Sci. USA, 116, 6641-6646,
635 https://doi.org/10.1073/pnas.1810774116, 2019.

Roldin, P., Ehn, M., Kurtén, T., Olenius, T., Rissanen, M. P., Sarnela, N., Elm, J., Rantala, P., Hao, L., and Hyttinen, N.: The role of highly oxygenated organic molecules in the Boreal aerosol-cloud-climate system, Nat. Commun., 10, 4370, https://doi.org/10.1038/s41467-019-12338-8, 2019.

Schell, B., Ackermann, I. J., Hass, H., Binkowski, F. S., and Ebel, A.: Modeling the formation of secondary organic
640 aerosol within a comprehensive air quality model system, J. Geophys. Res.-Atmos., 106, 28275-28293, https://doi.org/10.1029/2001jd000384, 2001.

Simoneit, B. R. T.: Biomass burning - a review of organic tracers for smoke from incomplete conbustion, Appl. Geochem., 17, 129-162, https://doi.org/10.1016/S0883-2927(01)00061-0, 2002.

Solomon, P. A., Crumpler, D., Flanagan, J. B., Jayanty, R. K., Rickman, E. E., and McDade, C. E.: U.S. national
645 PM$_{2.5}$ Chemical Speciation Monitoring Networks-CSN and IMPROVE: description of networks, J. Air Waste Manag. Assoc., 64, 1410-1438, https://doi.org/10.1080/10962247.2014.956904, 2014.

Song, M., Liu, P. F., Hanna, S. J., Li, Y. J., Martin, S. T., and Bertram, A. K.: Relative humidity-dependent viscosities of isoprene-derived secondary organic material and atmospheric implications for isoprene-dominant forests, Atmos. Chem. Phys., 15, 5145-5159, https://doi.org/10.5194/acp-15-5145-2015, 2015.

650 Srivastava, D., Vu, T. V., Tong, S., Shi, Z., and Harrison, R. M.: Formation of secondary organic aerosols from anthropogenic precursors in laboratory studies, npj Clim. Atmos. Sci., 5, https://doi.org/10.1038/s41612-022-00238-6, 2022.

Strader, R., Lurmann, F., and Pandis, S. N.: Evaluation of secondary organic aerosol formation in winter, Atmos. Environ., 33, 4849-4863, https://doi.org/10.1016/S1352-2310(99)00310-6, 1999.

655 Sun, P., Farley, R. N., Li, L., Srivastava, D., Niedek, C. R., Li, J., Wang, N., Cappa, C. D., Pusede, S. E., Yu, Z., Croteau, P., and Zhang, Q.: PM$_{2.5}$ composition and sources in the San Joaquin Valley of California: A long-term study using ToF-ACSM with the capture vaporizer, Environ. Pollut., 292, 118254, https://doi.org/10.1016/j.envpol.2021.118254, 2022.

Surratt, J. D., Kroll, J. H., Kleindienst, T. E., Edney, E. O., Claeys, M., Sorooshian, A., Ng, N. L., Offenberg, J. H.,
660 Lewandowski, M., Jaoui, M., Flagan, R. C., and Seinfeld, J. H.: Evidence for Organosulfates in Secondary Organic Aerosol, Environ. Sci. Technol., 41, 517-527, https://doi.org/10.1021/es062081q, 2007.

Tolocka, M. P., Jang, M., Ginter, J. M., Cox, F. J., Kanmens, R. M., and Johnston, M. V.: Formation of Oligomers in Secondary Organic Aerosol, Environ. Sci. Technol., 38, 1428-1434, https://doi.org/10.1021/es035030r 2004.

Turpin, B. J. and Huntzicker, J. J.: Identification of secondary organic aerosol episodes and quantification of
665 primary and secondary organic aerosol concentration during SCAQS, Atmos. Environ., 29, 3527-3544, https://doi.org/10.1016/1352-2310(94)00276-Q, 1995.

Vasilakos, P., Hu, Y., Russell, A., and Nenes, A.: Determining the Role of Acidity, Fate and Formation of IEPOX-Derived SOA in CMAQ, Atmosphere, 12, https://doi.org/10.3390/atmos12060707, 2021.

Volkamer, R., Ziemann, P. J., and Molina, M. J.: Secondary Organic Aerosol Formation from Acetylene (C$_2$H$_2$):
670 seed effect on SOA yields due to organic photochemistry in the aerosol aqueous phase, Atmos. Chem. Phys., 9, 1907-1928, https://doi.org/10.5194/acp-9-1907-2009, 2009.

Winkler, S. L., Anderson, J. E., Garza, L., Ruona, W. C., Vogt, R., and Wallington, T. J.: Vehicle criteria pollutant (PM, NO$_x$, CO, HCs) emissions: how low should we go?, npj Clim. Atmos. Sci., 1, 26, https://doi.org/10.1038/s41612-018-0037-5, 2018.

675 Xavier, C., Rusanen, A., Zhou, P., Dean, C., Pichelstorfer, L., Roldin, P., and Boy, M.: Aerosol mass yields of selected biogenic volatile organic compounds – a theoretical study with nearly explicit gas-phase chemistry, Atmos. Chem. Phys., 19, 13741-13758, https://doi.org/10.5194/acp-19-13741-2019, 2019.

Yang, Z., Tsona, N. T., Li, J., Wang, S., Xu, L., You, B., and Du, L.: Effects of NO$_x$ and SO$_2$ on the secondary organic aerosol formation from the photooxidation of 1,3,5-trimethylbenzene: A new source of organosulfates, Environ. Pollut., 264, 114742, https://doi.org/10.1016/j.envpol.2020.114742, 2020.

Yao, L., Li, X.-R., Guo, X.-Q., Liu, X.-R., and Wang, Y.-S.: Pollution characteristics of n-alkanes in atmospheric fine particles during Spring Festival of 2007 in Beijing, Huanjing Kexue/Environmental Science, 30, 589-593, 2009.

Young, D. E., Kim, H., Parworth, C., Zhou, S., Zhang, X., Cappa, C. D., Seco, R., Kim, S., and Zhang, Q.: Influences of emission sources and meteorology on aerosol chemistry in a polluted urban environment: results from DISCOVER-AQ California, Atmos. Chem. Phys., 16, 5427-5451, https://doi.org/10.5194/acp-16-5427-2016, 2016.

Yu, K. A., McDonald, B. C., and Harley, R. A.: Evaluation of Nitrogen Oxide Emission Inventories and Trends for On-Road Gasoline and Diesel Vehicles, Environ. Sci. Technol., 55, 6655-6664, https://doi.org/10.1021/acs.est.1c00586, 2021a.

Yu, Z., Jang, M., and Madhu, A.: Prediction of Phase State of Secondary Organic Aerosol Internally Mixed with Aqueous Inorganic Salts, J. Phys. Chem. A, 125, https://doi.org/10198-10206, 10.1021/acs.jpca.1c06773, 2021b.

Yu, Z., Jang, M., Zhang, T., Madhu, A., and Han, S.: Simulation of Monoterpene SOA Formation by Multiphase Reactions Using Explicit Mechanisms, ACS Earth Space Chem., https://doi.org/10.1021/acsearthspacechem.1c00056, 2021c.

Yu, Z., Jang, M., Kim, S., Son, K., Han, S., Madhu, A., and Park, J.: Secondary organic aerosol formation via multiphase reaction of hydrocarbons in urban atmospheres using CAMx integrated with the UNIPAR model, Atmos. Chem. Phys., 22, 9083-9098, https://doi.org/10.5194/acp-22-9083-2022, 2022.

Zaveri, R. A., Shilling, J. E., Fast, J. D., and Springston, S. R.: Efficient Nighttime Biogenic SOA Formation in a Polluted Residual Layer, J. Geophys. Res.-Atmos., 125, https://doi.org/10.1029/2019jd031583, 2020.

Zhang, H., Yee, L. D., Lee, B. H., Curtis, M. P., Worton, D. R., Isaacman-VanWertz, G., Offenberg, J. H., Lewandowski, M., Kleindienst, T. E., Beaver, M. R., Holder, A. L., Lonneman, W. A., Docherty, K. S., Jaoui, M., Pye, H. O. T., Hu, W., Day, D. A., Campuzano-Jost, P., Jimenez, J. L., Guo, H., Weber, R. J., de Gouw, J., Koss, A. R., Edgerton, E. S., Brune, W., Mohr, C., Lopez-Hilfiker, F. D., Lutz, A., Kreisberg, N. M., Spielman, S. R., Hering, S. V., Wilson, K. R., Thornton, J. A., and Goldstein, A. H.: Monoterpenes are the largest source of summertime organic aerosol in the southeastern United States, P. Natl. Acad. Sci. USA, 115, 2038-2043, https://doi.org/10.1073/pnas.1717513115, 2018.

Zhang, J., He, X., Gao, Y., Zhu, S., Jing, S., Wang, H., Yu, J. Z., and Ying, Q.: Assessing Regional Model Predictions of Wintertime SOA from Aromatic Compounds and Monoterpenes with Precursor-specific Tracers, Aerosol Air Qual. Res., 21, https://doi.org/10.4209/aaqr.210233, 2021.

Zhang, X., McVay, R. C., Huang, D. D., Dalleska, N. F., Aumont, B., Flagan, R. C., and Seinfeld, J. H.: Formation and evolution of molecular products in alpha-pinene secondary organic aerosol, P. Natl. Acad. Sci. USA, 112, 14168-14173, https://doi.org/10.1073/pnas.1517742112, 2015.

Zheng, B., Tong, D., Li, M., Liu, F., Hong, C., Geng, G., Li, H., Li, X., Peng, L., Qi, J., Yan, L., Zhang, Y., Zhao, H., Zheng, Y., He, K., and Zhang, Q.: Trends in China's anthropogenic emissions since 2010 as the consequence of clean air actions, Atmos. Chem. Phys., 18, 14095-14111, https://doi.org/10.5194/acp-18-14095-2018, 2018.

715   Zhou, C., Jang, M., and Yu, Z.: Simulation of SOA formation from the photooxidation of monoalkylbenzenes in the presence of aqueous aerosols containing electrolytes under various NO_x levels, Atmos. Chem. Phys., 19, 5719-5735, https://doi.org/10.5194/acp-19-5719-2019, 2019.

Table 1. List of SOA precursors and SOA species in the UNIPAR model.

Type of precursors	UNIPAR species name (OMH, OMP)[a]	Hydrocarbons	Stoichiometric coefficient (α_i)[b]	Unified physico-chemical parameters (MW_i, $O:C_i$, and HB_i)	SOA data	Regional simulation
Aromatics	OMH_AR OMP_AR	Benzene	50×4	50	(Im et al., 2014; Zhou et al., 2019)	(Yu et al., 2022)
		Toluene	50×4			
		Ethylbenzene	50×4			
		Propylbeneze	50×4			
		o-Xylene	50×4			
		m-Xylene	50×4			
		p-Xylene	50×4			
		123-trimethylbenzene	50×4			
		124-trimethylbenzene	50×4			
		135-trimethylbenzene	50×4			
Alkanes	OMH_AK OMP_AK	Alkane (C9–C14)	50×4	50	(Madhu et al., 2022)	This study
		Alkane (C15–C19)	50×4			
		Alkane (C20–C24)	50×4			
Terpene	OMH_TE OMP_TE	Terpene with OH radicals	50×4	50	(Yu et al., 2021c; Han and Jang, 2023)	This study
		Terpene with ozone	50×4			
		Terpene with nitrate radicals	50×4		(Han and Jang, 2023)	
Sesquiterpene	OMH_SP OMP_SP	Sesquiterpene with OH radicals	50×4	50	(Han and Jang, 2023)	This study
		Sesquiterpene with ozone	50×4			
		Sesquiterpene with nitrate radicals	50×4			
Isoprene	OMH_IS OMP_IS	Isoprene with OH radicals	51×4	51	(Beardsley and Jang, 2016; Han and Jang, 2023)	This study
		Isoprene with ozone	51×4			
		Isoprene with nitrate radicals	51×4		(Han and Jang, 2023)	

720 [a] OMH is the SOA mass heterogeneously formed and OMP is that produced via multiphase partitioning.
[b] Four different mathematical equation sets for α_i. For aromatics and alkanes, the mathematical equation sets for α_i include 'Low NO$_x$-Fresh', 'Low NO$_x$-Aged', 'High NO$_x$-Fresh', and 'High NO$_x$-Aged'. For terpene, sesquiterpene, and isoprene, the mathematical equation sets for α_i include 'Low NO$_x$-Daytime', 'Low NO$_x$-Nighttime', 'High NO$_x$-Daytime', and 'High NO$_x$-Nighttime'.
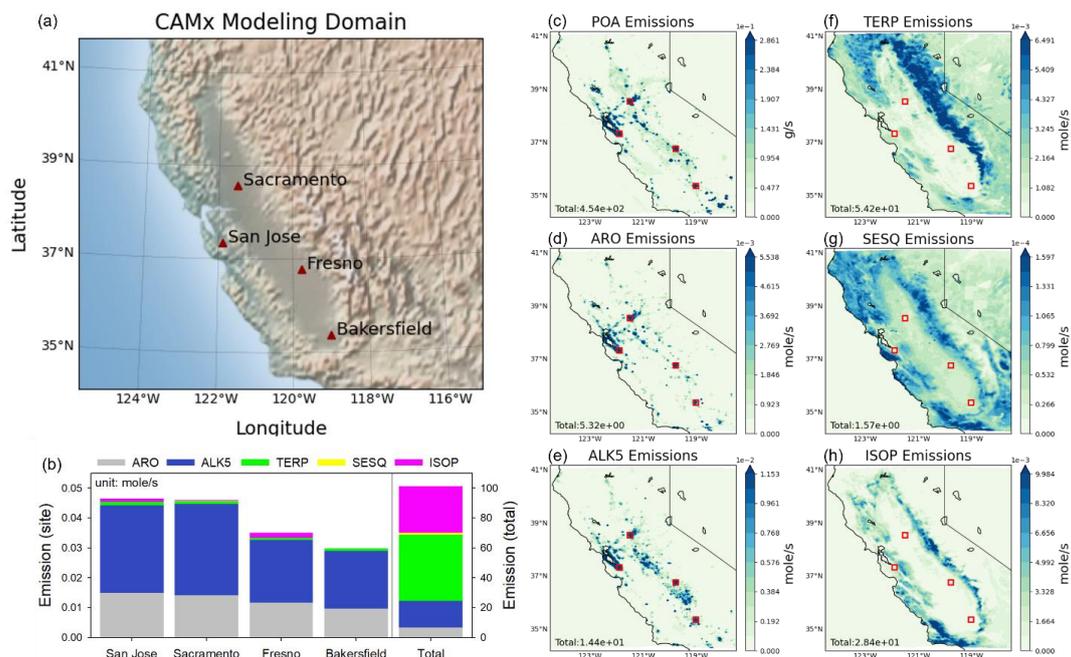
725

Table 2. List of observation sites.

	San Jose	Sacramento	Fresno	Bakersfield
Latitude	37.35	38.61	36.79	35.36
Longitude	-121.89	-121.37	-119.77	-119.06
Elevation (above MSL)	31m	8m	96m	0m
Local Type	Urban and Center City	Suburban	Urban and Center City	Urban and Center City
Geography	The San Francisco Bay Area Air Basin (SFBAAB or Bay Area)		The Central Valley	

Fig. 1. The structure of the CAMx model integrated with UNIPAR to form SOA via multiphase reactions of hydrocarbons.

730

Fig. 2. (a) The CAMx modeling domain and selected observation sites in this study. (b) The amount of major SOA precursors emission for each site and the total of the domain. (c–h) Spatial distributions of POA and major SOA precursors emission. The emission data is SAPRC07-based and averaged from January to February 2018. ARO is the sum of benzene, toluene, *o*-xylene, *p*-xylene, *m*-xylene, and 1,2,4-trimethylbenzene.

735
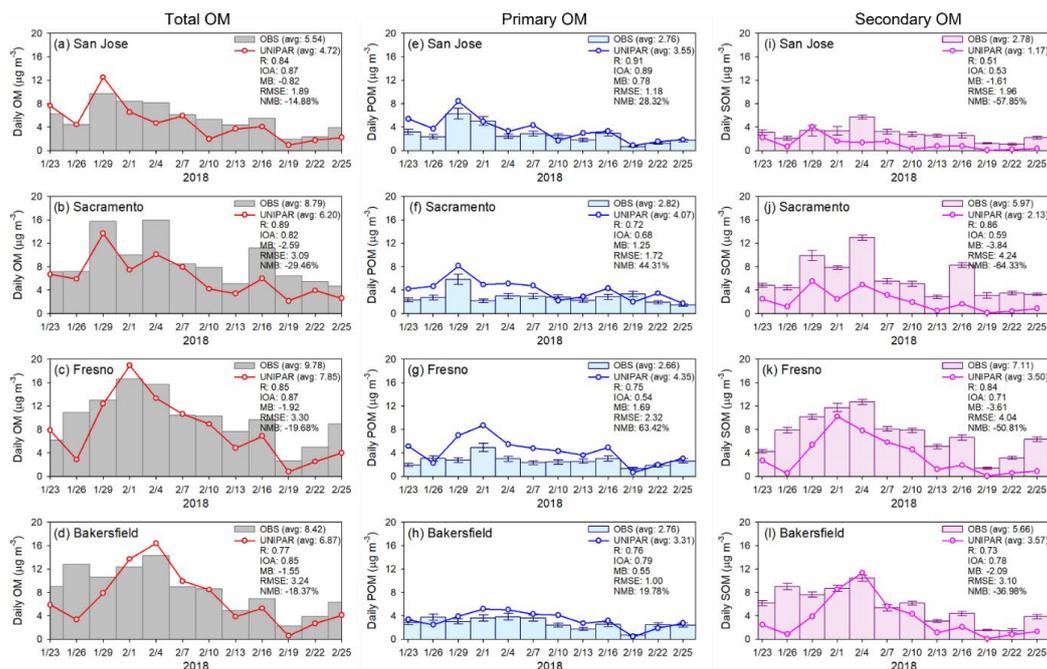
Fig. 3. (a–d) Time series of observed and simulated total OM mass concentration (µg m^{-3}) at the CSN (Chemical Speciation Network) sites selected in this study. **(e–h)** Time series of observed POA and simulated POA. **(i–l)** Time series of observed SOA and simulated SOA. Vertical bars represent observed POA and SOA estimated using a value of 2.4 for the POC/EC ratio, while the error bars represent a range of POC/EC ratio from 2.05 to 2.75. The OM mass concentrations are displayed in a daily averaged value every three days since the CSN sites operate on a 1-in-3-day sample collection schedule. The equations for statistical parameters are described in Table S8. R is correlation coefficient, IOA is Index of Agreement, MB is Mean Bias, RMSE is Root Mean Square Error, and NMB is Normalized Mean Bias.

740

745
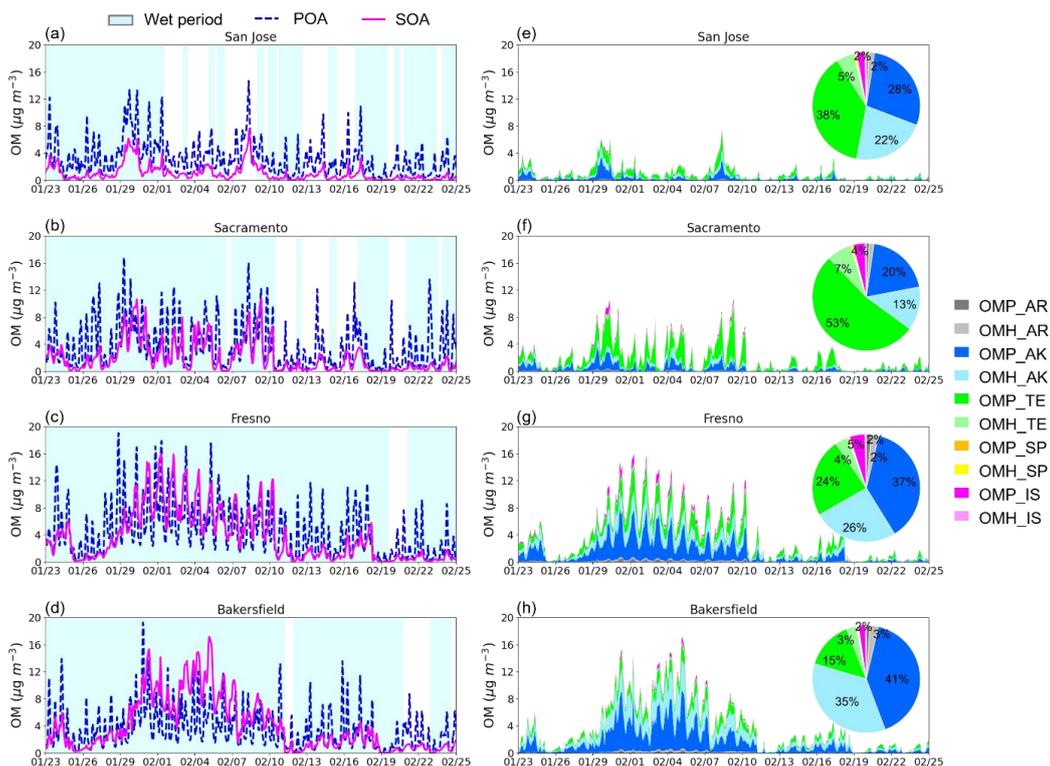
Fig. 4. (a–d) Time series of simulated POA, SOA, and salted aerosol phase state (wet and dry). (e–h) Time series of simulated SOA species in the UNIPAR model at each site and the pie charts to represent the fraction of SOA species associated with graphs (e–h).
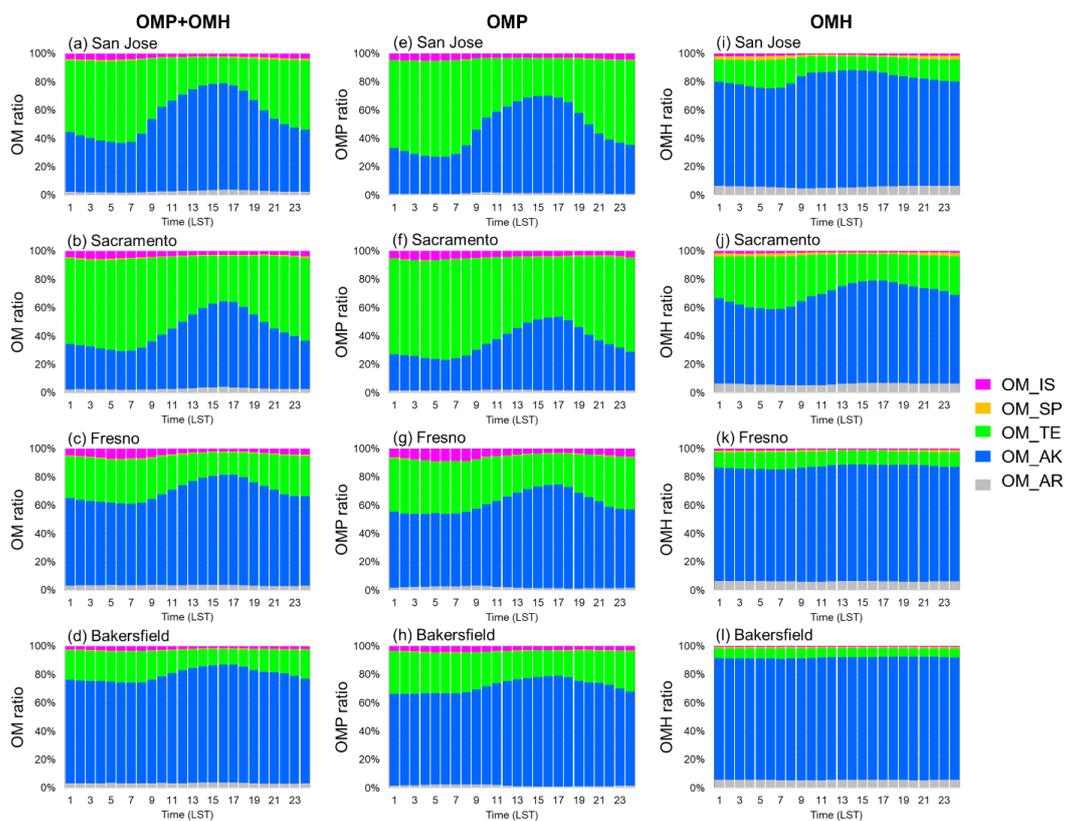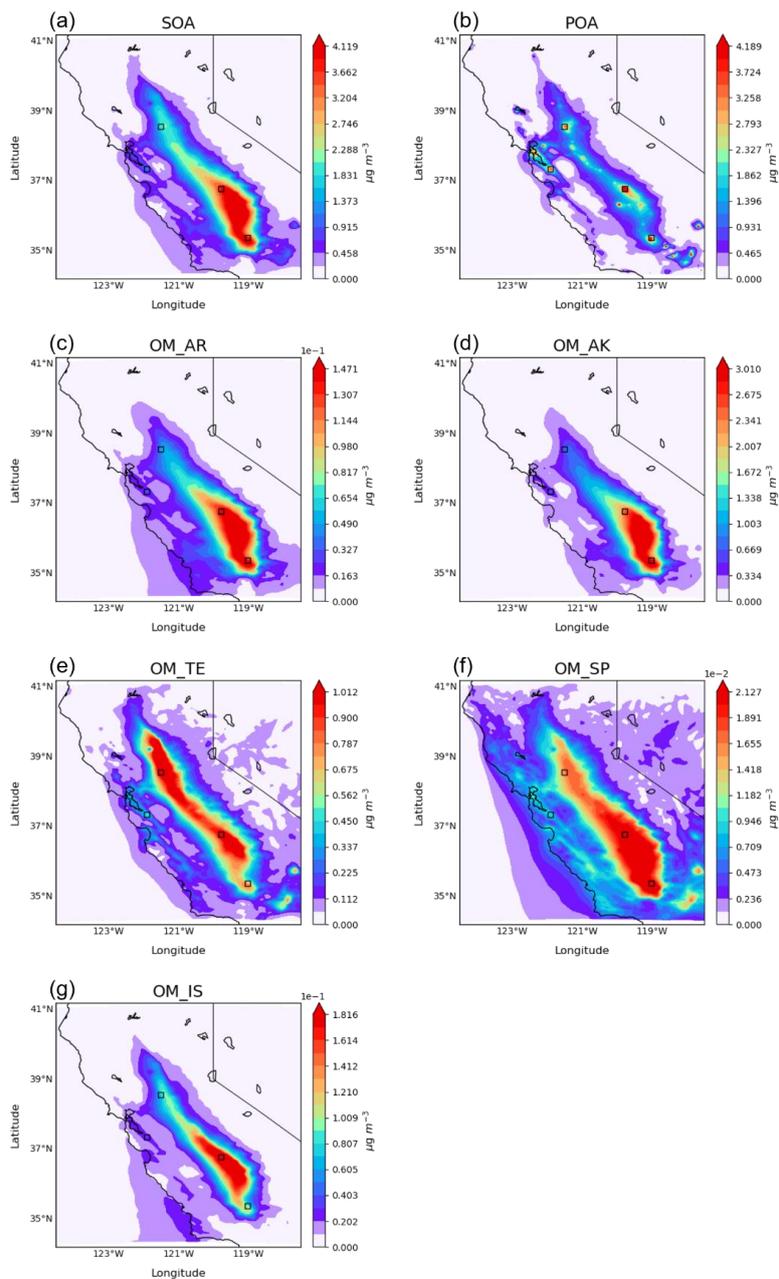
750

Fig. 5. Averaged diurnal variation of (a–d) the total SOA (OMP + OMH) species, (e–h) the OMP SOA species, and (i–l) the OMH SOA species during the simulation period (01/23/2018-02/24/2018).

Fig. 6. Spatial distribution of (a) total SOA, (b) POA, (c) aromatic SOA (OMP_AR+OMH_AR), (d) alkane SOA (OMP_AK+OMH_AK), (e) terpene SOA (OMP_TE+OMH_TE), (f) sesquiterpene SOA (OMP_SP+OMH_SP), and (g) isoprene SOA (OMP_IS+OMH_IS). The simulation results at the surface level were averaged between 01/23/2018 and 02/24/2018.
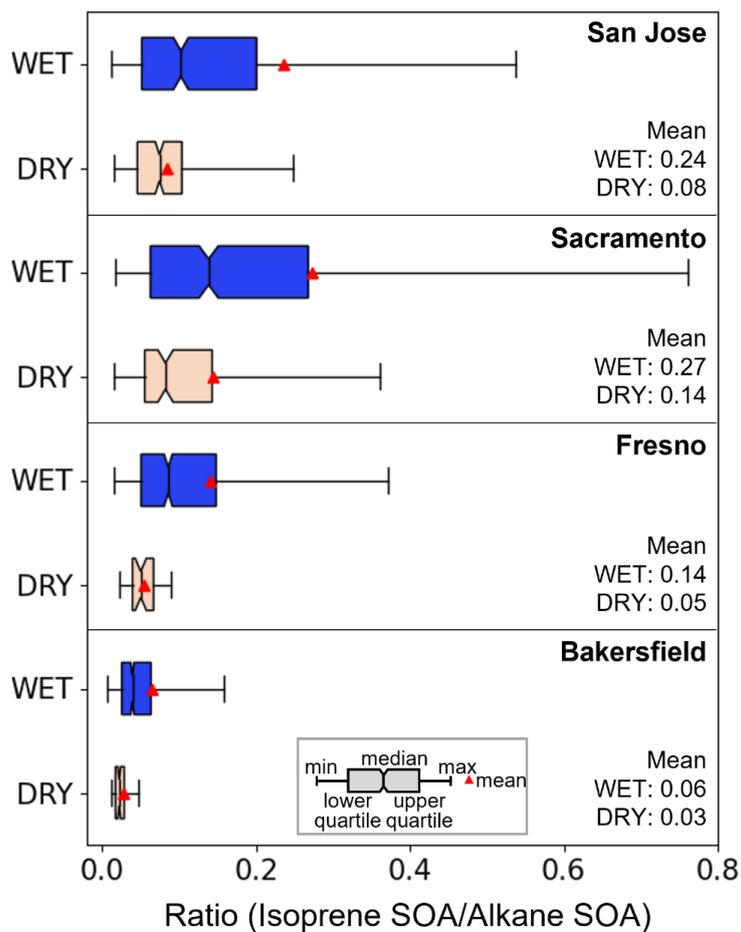
755

760

Fig. 7. The mass ratio of isoprene SOA to alkane SOA at the San Jose, Fresno, Sacramento, and Bakersfield during the wet and dry periods.